PdZn catalysts for CO_2 hydrogenation to methanol using chemical vapour impregnation (CVI)

H. Bahruji,[a] M. Bowker,[a,b*] W. Jones[b], J. Hayward,[a] J. Ruiz Esquius,[a] D. J. Morgan[a] and G. J. Hutchings[a]

Abstract

The formation of PdZn bimetallic alloys on ZnO, TiO_2 and Al_2O_3 supports was investigated, together with the effect of the alloy formation on the CO_2 hydrogenation reaction. The chemical vapour impregnation (CVI) method produced PdZn nanoparticles with diameters of 3-6 nm. X-ray photoelectron spectroscopy and X-ray diffraction revealed the changes in structure of the PdZn alloy that helps stabilise formate intermediates during methanol synthesis. PdZn supported on TiO_2 exhibits high methanol productivity of 1730 mmol $kg_{cat}^{-1}h^{-1}$ that is associated with the high dispersion of the supported PdZn alloy.

Introduction

In recent years the effects of global warming have attracted efforts to tackle the rising level of CO_2 in the atmosphere by the capture, storage and utilisation of this abundant carbon source. One such effort is the transformation of CO_2 into methanol. Olah *et al*. introduced the anthropogenic carbon cycle concept for utilising carbon dioxide for synthetic hydrocarbon products[1]. In this concept methanol is used as a green starting chemical for the synthesis of fuels and various of synthetic hydrocarbon products, and therefore CO_2 conversion to methanol is a crucial initial step[1]. However, the thermodynamic stability of CO_2 means that significant amounts of energy are required for activation and conversion into value-added products. The choice of catalysts is important to provide active sites for C-O bond dissociation and H-insertion in order to ensure high yields of methanol. For the methanol synthesis to be considered green, the captured CO_2 has to combine with H_2 produced from a sustainable source.

The first commercial methanol synthesis have been carried out since 1920s using ZnO/Cr_2O_3 catalyst[2]. Cr_2O_3 was added to ZnO to improve catalytic activity and prolong the life of the catalyst. Currently $Cu/ZnO/Al_2O_3$ catalyst developed by ICI have been used for methanol synthesis using a mixture of CO_2, CO and H_2 as feedstock[2, 3]. The reaction was carried out at 50 - 100 bar and 200-300 °C. Studies on Cu catalysts concluded that the methanol productivity was strongly correlated with the specific surface area of Cu[4], with Cu oxidation states[5] and the Cu-Zn interface[6, 7] also being significant factors. Cu-Zn species possess a bifunctional catalytic property which is created through interaction between Cu and ZnO in close proximity[8]**.** Deactivation over time is observed mainly due to the sintering of Cu metal[9]. Among the catalysts that have the potential for CO_2 hydrogenation, Pd has attracted interest due to the property malleability derived from the presence of a nearly full d-band. Pd/ZnO has higher stability than Cu catalysts for the methanol steam reforming reaction[10, 11]. We previously found that Pd/ZnO catalysts can be active for CO_2 hydrogenation to methanol with the choice of preparation method and Pd precursor affecting the selectivity of the products [12]. The catalytic activity of Pd is strongly associated with the type of metal oxide support including ZnO[13-15], CeO_2[16] and Ga_2O_3[17-19]. Pd has a strong inclination to form intermetallic species with the ZnO when exposed at high temperature under a reducing environment[20]. Pd/ZnO transformed into PdZn alloy under a reducing environment which subsequently altered the course of catalytic reaction to favour methanol production over the reverse water gas shift reaction[12]. For the CO_2 hydrogenation reactions, the proximity between metal and substrate stabilized the intermediate formate species, which is reported as the intermediate on Cu-Zn[21] and PdZn alloy[12]. In Cu-Zn systems, the formate intermediate can only be effectively converted to methanol on Cu-Zn surface but not on Cu alone[22]. The hydrogenation of formate occurs at temperature below its decomposition which subsequently allows for complete hydrogenation to methanol[23].

As in many heterogeneous catalytic systems, the dispersion of metal nanoparticles is important for enhancing the number of active sites. The prevention of highly dispersed catalysts from area loss by sintering is a challenging task, and researchers are conducting investigations into new catalytic preparation methods that improve nanoparticle dispersion and stability. The chemical vapor impregnation (CVI) method has been previously studied for nanoparticle deposition and can produce high metal

dispersion on support materials[24-26]. In this method an organometallic precursor is heated under reduced pressure to induce sublimation, but not at sufficient temperatures to cause decomposition. In this manner the organometallic is introduced from the gas phase and is adsorbed on the metal oxide support and tends to form highly isolated metal nuclei. This method also has the potential to enable the tailoring of the composition and morphology of supported nanoparticles in an easily accessible and scalable manner [26]. In the CVI method, the precursor sublimation step and deposition onto the support are not spatially separated since the precursor and support are in intimate contact during the sublimation–deposition step. Studies previously reported on Pd and Pt nanoparticles deposited *via* the CVI method onto TiO_2 reveals narrow particle size distributions of 1.5-2.8 nm[24, 26].

Previous investigations into the reactivity of Pd/ZnO catalysts for CO_2 hydrogenation reaction found that the activity of the catalyst is strongly influenced by the method of catalyst preparation, the type of palladium precursor, and the annealing treatment of the catalyst[12]. In that work we compared the behavior of materials produced by incipient wetness impregnation and sol immobilization methods. Here we report the activity of Pd catalysts on ZnO, TiO_2 and Al_2O_3 supports to clarify the importance of the formation of the Pd-Zn alloy and the catalysts were synthesized using the CVI method with non-chloride palladium precursors. This is important to eliminate the chlorine poisoning which can occur[4]. Chloride poisoning has been shown to promote particle agglomeration and shift the products towards a reverse water gas shift reaction[12].

Experimental

Chemical Vapour Impregnation (CVI) preparation

Catalysts were prepared using a CVI method based on previous work by Forde *et al*[26]. This method was chosen in part to avoid the use of solvents and chloride precursors, and in part for the highly dispersed metal species it produces. For 5 % Pd catalysts, ZnO, TiO_2 or Al_2O_3 and palladium acetylacetonate ($Pd(acac)_2$) were placed into glass vial and mixed thoroughly. This mixture was then transferred to a 50 ml Schlenk flask with the tube sealed. The tube was connected to a Schlenk line and was evacuated at room temperature (~10^{-3} mbar). The mixture was heated at 145 °C for 1 hour. For PdZn catalysts, zinc acetylacetonate ($Zn(acac)_2$) was added to the initial precursor mixture at Pd:Zn atomic ratios of 1:1 to 1:10, followed by a similar procedure. The sample was calcined in air at 500 °C for 16 hours to decompose the acetylacetonate precursors.

Catalyst Characterisation

The characterisation of the samples was performed using a range of techniques. Powder X-ray diffraction (PXRD) patterns were obtained at room temperature with an Enraf Nonus FR590 diffractometer fitted with a hemispherical analyzer, using Cu Kα radiation (λ=1.54 Å). X-ray photoelectron spectra (XPS) were recorded on a Kratos Axis Ultra-DLD XPS spectrometer with a monochromatic Al kα source (75-150 W) and analyser pass energies of 160 eV (for survey scans) or 40 eV (for detailed scans). Samples were mounted using a double-sided adhesive tape and binding energies referenced to the C (1s) binding energy of adventitious carbon contamination which was taken to be 284.7 eV. Data were analyzed using Casa XPS software [27].

To provide detailed morphological and compositional information at micro and nano-scales, high-resolution transmission electron microscope (HRTEM) system JEOL 2100 (LaB6) is employed. For the analysis, the material was ground and mixed with water was placed on the TEM grid and dried. The instrument is equipped with a high-resolution Gatan digital camera (2k x 2k) with a maximum resolution of 0.2 Å giving us the ability to see crystal lattices, to obtain diffraction patterns and giving accurate measurement of the lattice d spacing utilising Digital Micrograph software. In scanning transmission electron microscopy (STEM) mode, dark field a HAADF/Z-contrast detector was used to provide excellent compositional contrast. An energy dispersive X-ray spectrometer (EDS) system (Oxford Instruments), was equipped with a large-area 80 mm^2 SDD (Silicon Drift Detector). X-MaxN 80 T was employed for the elemental analysis in line scans, and elemental mapping modes.

Catalytic testing

The catalytic performance of the catalysts for CO_2 hydrogenation was determined in a fixed-bed continuous-flow reactor. A catalyst (0.5 g, 425-500 µm) was placed in a stainless tube reactor with i.d. of 0.5 cm and length 50 cm with the catalysts packed

in the middle of the tube, occupying a length of ~ 10 cm. Prior to the reaction, catalysts were pre-reduced in a flow of 5 % H_2/Ar gas (30mL/min) for 1 h at 400°C under atmospheric pressure. The reactor was cooled to 250 °C and a mixture of CO_2 and H_2 gases, (1 CO_2: 3 H_2 molar ratios) was introduced with a flow rate of 30 mL min^{-1}. The pressure was increased to 20 bar using a back-pressure valve. All the post-reactor lines and valves were heated at 130 °C to avoid product condensation. The gas products were analysed *via* online gas chromatography using an Agilent 7890 system with an FID and TCD. Nitrogen was used as an internal standard. Reported values are given after 3 h of reaction under steady state unless otherwise stated.

Results

Catalyst characterization

XRD analysis

Catalysts were primarily characterized using X-ray diffraction (XRD) analysis to gain information about PdZn formation. Previous studies on Pd/ZnO catalysts revealed that PdZn alloy was formed under H_2 at 200 °C but achieved high methanol productivity when pre-reduced at 400 °C[12]. Figure S1-S3 shows (supplementary) the XRD patterns of 5% Pd/ZnO, 5% Pd:Zn (1:10)/TiO_2 and 5% Pd:Zn (1:10)/Al_2O_3. Maud analysis software[28] has been used to resolve the XRD peak into different components. Detailed characterisation of the catalysts using XRD reveals that the tetragonal β-PdZn phase alloy was formed on ZnO and TiO_2 as seen by the peaks appearing at 41° and 44°, and only β-PdZn (111) was clearly seen on Al_2O_3. The intensity of the peak varied on the different supports. The peaks corresponding to ZnO and the PdZn alloy were observed on 5% Pd:Zn (1:10)/TiO_2 and 5% Pd:Zn (1:10)/Al_2O_3 catalysts, implying that some of the Zn precursor was reduced to form the alloy meanwhile some of the Zn was oxidised to ZnO during calcination. Based on the intensity of the ZnO peaks at 31.7, 34.4, 36.2, 47.5, 66, 68 and 69°, 5% Pd:Zn (1:10)/TiO_2 shows less crystalline ZnO in the structure in comparison to 5% Pd:Zn (1:10)/Al_2O_3.

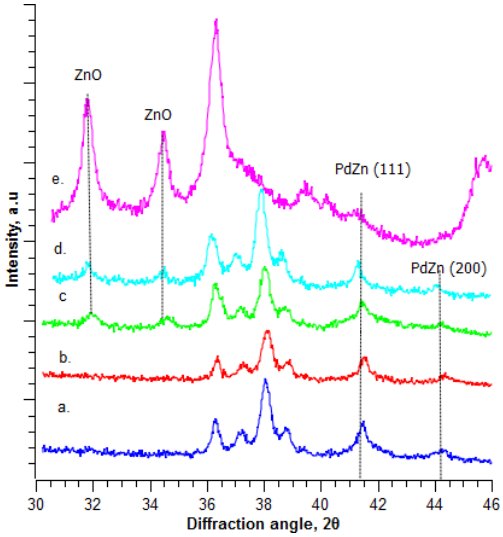

Fig 1. X-ray diffraction pattern for a. 5% Pd:Zn (1:1)/TiO_2, b. 5% Pd:Zn (1:2)/TiO_2; c. 5% Pd:Zn (1:5)/TiO_2 ; d. 5% Pd:Zn (1:10)/TiO_2 and e. 5% Pd:Zn (1:10)/Al_2O_3. All the catalysts were calcined in air at 500°C for 16h followed by reduction in 5% H_2/Ar at 400°C

Figure 1 shows XRD patterns for the PdZn catalysts on TiO_2 with varied Pd:Zn molar ratios (a-d) and 5% Pd:Zn (1:10)/Al_2O_3 (e) at diffraction angles of 30° – 46°. For all of the catalysts, the PdZn peak at 41° (111) was clearly visible, but the peak at 44° (200) was only apparent for PdZn on the TiO_2 support, but not on Al_2O_3. At low Pd:Zn molar ratios (1:1 and 1:2), no peaks corresponding to ZnO were observed, indicating that the ZnO precursor was reduced to form PdZn alloy. For high Pd:Zn ratios (1:5 and 1:10) the ZnO peaks were observed at diffraction angles of 32° and 34°.

XPS and XAES

XPS analysis was used to investigate the formation of the PdZn alloy and the level of carbon impurities on the catalyst surface. In what follows it's important to note that the samples have been exposed to air prior to XPS analysis. As is well known

this can lead to surface contamination by carbonaceous species, and may lead to oxidation of reduced species, and we will consider these effects below.

Annealing the as-synthesised catalyst in air or hydrogen significantly affects catalytic activity, as reported below. The 5% Pd/ZnO catalyst was separately treated in air and in hydrogen and was characterised using XPS analysis. The carbon 1s spectra were used to determine the level of carbon contamination from acetylacetonate decomposition on the surface. Figure 2(i) reveals the effect of two different treatments on the level of surface carbon in the 5% Pd/ZnO catalyst. A significant decrease in the intensity of the C 1s signal was observed when the catalyst was first subjected to air calcination at 500 °C, followed by reduction when compared to treatment in hydrogen alone. The observation was also supported by the carbon content from wide survey XPS analysis (supporting information fig S4). The quantification of the C 1s peak shows 73 % of carbon on the catalysts that was only subjected to reduction at 400 °C, compared to only 37 % of on the catalysts that were calcined at 500 °C. Whilst carbon contamination is inevitable after exposure of such samples to air, it is clear that calcination in static air managed to remove a significant amount of the carbon. This has an effect on the activity of 5 % Pd/ZnO catalysts as discussed below. Figure 2(ii) also shows the XPS O 1s spectra of the catalysts. The O 1s signal shows peaks at 531 eV and 532.5 eV that corresponded to ZnO and ZnOH respectively. However, for 5% Pd/ZnO that has only been subjected to reduction in H_2 at 400^{o}C, it shows a significant broadening of ZnOH peak ~ 532.5 to high binding energy. This is probably due to the formation of carbonate species on the surface during acetylacetonate decomposition that has not completely removed during the annealing treatment.

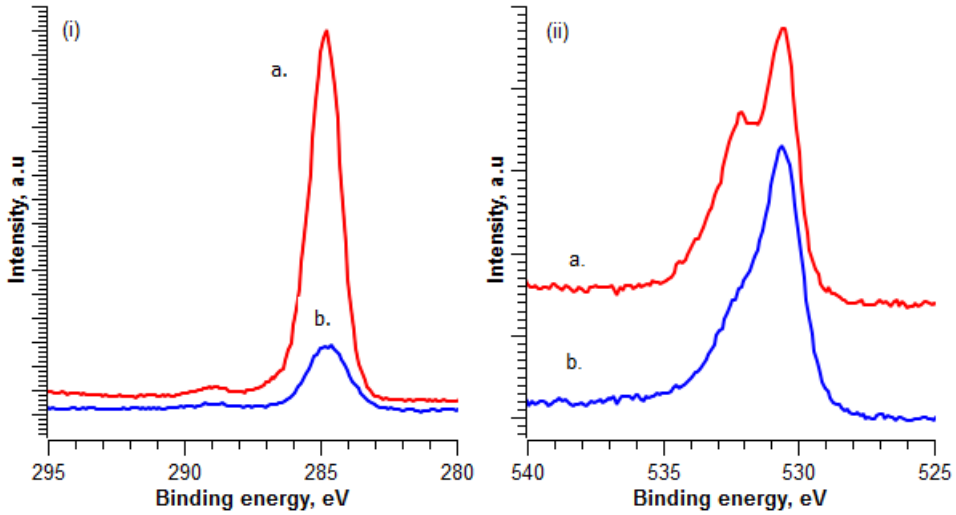

Fig. 2. (i) XPS C 1s spectra and (ii) O 1s spectra of a. 5% Pd/ZnO that was only treated under 5% H_2/argon at 400^{o}C for 3 hours; and b. 5% Pd/ZnO that was calcined in air at 500^{o}C for 16 h followed by reduction at 400^{o}C for 1h

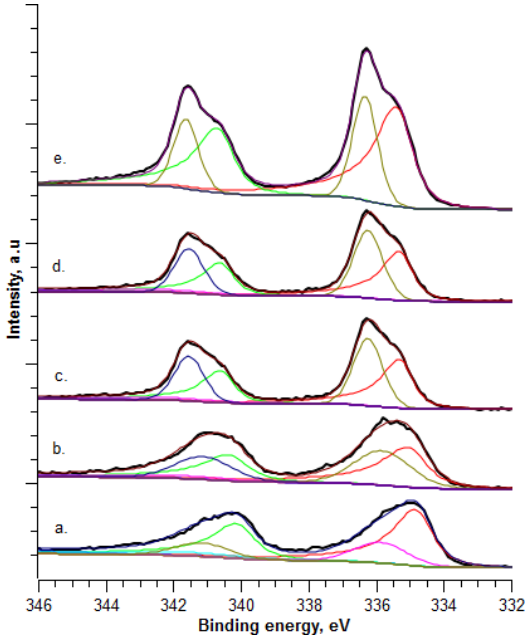

Fig. 3: XPS Pd 3d spectra of a. 5% Pd:Zn (1:1)/TiO_2, b. 5% Pd:Zn (1:2)/TiO_2; c. 5% Pd:Zn (1:5)/TiO_2 ; d. 5% Pd:Zn (1:10)/TiO_2 and e. 5% Pd:Zn (1:10)/Al_2O_3. All the catalysts were calcined in air at 500°C for 16h followed by reduction in 5% H_2/Ar at 400°C. Tabulated Pd 3d XPS data were given in Table S1.

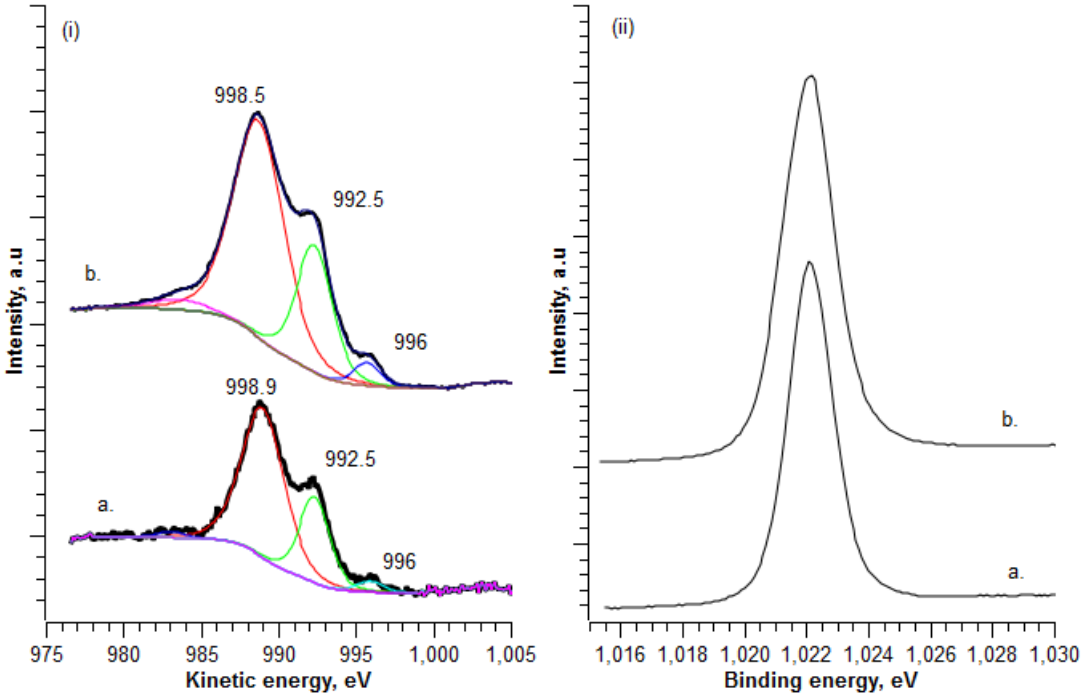

Fig. 4. (i) XPS Zn LMM auger electron spectra and (ii) XPS Zn $2p_{3/2}$ spectra of a. 5% Pd:Zn (1:5)/TiO_2 and b. 5% Pd:Zn (1:10)/Al_2O_3. All the catalysts were calcined in air at 500°C for 16h followed by reduction in 5% H_2/Ar at 400°C

The influence of Pd:Zn molar ratios on the formation of the PdZn alloy on TiO_2 support was investigated. Figure 3 shows XPS Pd 3d spectra of these materials. These catalysts were air calcined first, followed by reduction at 400 °C and revealed a peak at 335.0 eV binding energy, corresponding to Pd^0 with a shoulder peak at ~336.0 eV[20]. The peak at 336.0 eV corresponds to the formation of the PdZn alloy on the catalyst following reductive transfer of Zn from ZnO[29], although the Pd peak is still a dominant species for the 5% Pd:Zn (1:1)/TiO_2 sample. These shifts are probably caused by Pd (4d) → Zn (4p) charge transfer and a Pd (4d) → Pd (5s, 5p) rehybridization[30]. Further increasing the Pd:Zn ratios to 1:2, the intensity of PdZn peak at 336.1 eV is enhanced and becomes dominant at Pd:Zn 1:5. Although the XRD analysis confirmed the presence of the β-PdZn alloy in

PdZn deposited on TiO_2 catalysts, the alloy is formed when the Zn mole fraction is within the range of 0.4-0.6[31]. These results suggest that increasing the ratio of Pd:Zn in the preparation increases the amount of Zn that is incorporated into the Pd lattice and so may simultaneously enhance the amount of PdZn alloy on the surface.

In order to try to learn more about the alloying process we examined the Zn Auger spectra, since these may show changes in level structure better than the core levels of Zn. We have also measured the spectra of Zn metal, partially oxidised Zn metal in air at 80 ^oC and ZnO powder as reference. It is possible that the surface of the samples may become oxidised when exposed to air, especially when the surface has highly oxidisable species such as Zn^0. The Zn $L_3M_{24}M_{24}$ Auger electron spectra of these samples are shown in Fig. S5. For Zn metal it was reported that there are peak positions of 992 (major) and 996 (minor) [32], while for the oxide they are 988 and 991 respectively[33]. Zn metal shows major peaks at kinetic energy of 996 eV and 992.5 eV and minor peaks at 989.3 eV and 986 eV (fig. S5a). Apart from peaks at 996 eV and 992.5 eV that correspond to Zn metallic state, the presence of peaks at 998.9 eV and 986 eV implies a thin layer of oxidised Zn occurs on the metal surface. On partially oxidised Zn (fig. S5b), the metal peaks still visible at 996 eV and 992.5 eV meanwhile oxidised peak at 998.5 becomes broader. Analysis on ZnO powder reveals peak at 988 eV and a shoulder at 991 eV. The shoulder peak at 991 eV was suggested previously by Li et al as interstitial Zn present as defect sites in the ZnO lattice[33]. These changes between metallic and oxidised states are thus much clearer in the Auger spectra than in the core level spectra and reflect changes in the M (valence) levels of Zn.

As mentioned above, due to Zn is a highly oxidisable species, the only cases for these samples where we could definitely identify the presence of the Zn metal was for the 5% Pd:Zn (1:5)/TiO_2 and 5% Pd:Zn (1:10)/Al_2O_3 and these are shown in Fig 4(i). The equivalent core level Zn $2p_{3/2}$ XPS is shown in Fig 4(ii), revealing a similar binding energy of ~ 1022 eV for these samples. This is not surprising since the Zn 2p is less sensitive towards small ZnO reduction changes with only a small possible binding energy shift between Zn metal and ZnO [34, 35]. Significant shifts in Zn metal and ZnO positions can, however, be expected between the metal and oxide in the Auger LMM. The Auger indicates that most of the Zn in the structure exists as Zn^{2+} which most likely to be ZnO[36], but there is a shoulder peak at 992 eV, together with the fingerprint for the presence of the metal at 996 eV[32]. Besides that, the changes of shoulder peak in Zn Auger profile could be either due to the oxygen vacancies in ZnO or from metallic Zn[37, 38]. Similar observation are seen on Cu/ZnO/Al_2O_3 catalysts, which show increasing intensity of the 996 eV peak when the catalysts are reduced in H_2[37]. Studied by Deroubaix and Marcus on Zn $L_3M_{24}M_{24}$ Auger electron spectra of CuZn alloy showed a 0.3eV shift towards higher kinetic energy from Zn metal which less than the shift observed for ZnO – 3.9 eV[32]. We can conclude here that the 996 eV peak is from the metallic PdZn alloy whose presence is confirmed by the XRD shown above. It is very likely that a significant fraction of the Zn at the surface of these alloy nanoparticles is oxidised during transfer into the XP spectrometer, and hence the large signal seen for ZnO. It is interesting to note that though this is the case, there is little evidence for Pd oxidation, presumably due to protection from the Zn/ZnO at the surface. Indeed, maybe it is protected by a covering layer.

H_2-TPR analysis

The interactions between Pd, Zn and the oxide support were probed using H_2-TPR analysis (Fig 5). The catalysts were oxidised in air at 500 °C prior to the TPR experiment. The H_2-TPR analysis was also compared to 5% Pd/TiO_2 and 5% Pd/Al_2O_3 catalyst. The profile of 5% Pd/TiO_2 shows a negative peak at 107^{o}C due to decomposition of the β-Pd hydride species [39]. However, 5% Pd/Al_2O_3 only shows reduction peak of PdO at ~ 150^{o}C. The β-Pd hydride species formed through hydrogen adsorption or diffusion in the Pd^o crystallite[40]. This is a common feature of Pd/TiO_2 and the decomposition β-Pd hydride proves that the reduction of PdO occurred at temperature below this, probably before the temperature ramp. It has been reported that PdO reduces at 20^{o}C-50^{o}C and can occur during the initial flushing of the system [39].
The reduction of 5% Pd/ZnO and 5% Pd:Zn (1:10)/TiO_2 catalysts started at a similar temperature ~ 50 °C. The peak for 5% PdZn (1:10)/TiO_2 however centred at much lower temperature (~ 90 °C) than 5% Pd/ZnO. In contrast 5% Pd/ZnO shows two peaks centred at 90 and 140 °C, which suggest the presence of two different Pd species with different environments and interaction with the ZnO support. 5% Pd:Zn (1:10)/TiO_2 also shows a reduction peak at ~90 °C; significantly lower than 5% Pd/ZnO and 5% PdZn (1:10)/Al_2O_3 catalyst. It also loses its negative β-Pd hydride as shown in 5% Pd/TiO_2 catalyst. These suggest interaction between Zn and Pd on TiO_2 catalyst which may influence the catalytic performance. 5% Pd:Zn (1:10)/TiO_2 shows the most activity for CO_2 hydrogenation which suggests that Pd on this catalyst was in a close proximity with defect ZnO sites.

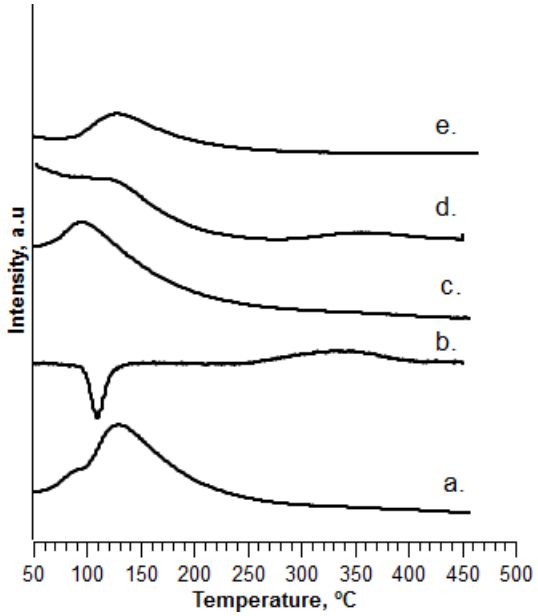

Fig. 5. H_2 TPR analysis of a. 5% Pd/ZnO; b. 5% Pd/TiO_2; c. 5% Pd:Zn (1:10)/TiO_2; d. 5% Pd/Al_2O_3, and e. 5% Pd:Zn (1:10)/Al_2O_3. All the catalysts were calcined in air at 500 °C before measurement.

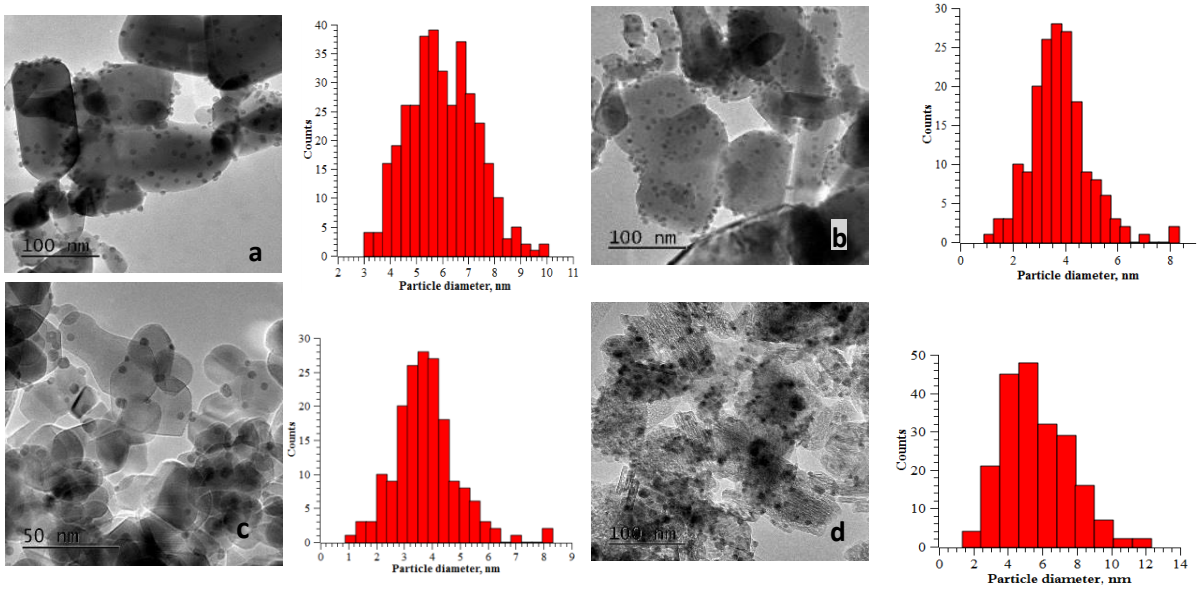

Fig. 6. TEM analysis and particle size distribution of a. 5% Pd/ZnO reduced in 5% H2/Ar at 400°C, b. 5% Pd/ZnO that was calcined at 500°C followed by reduction in 5% H2/Ar at 400°C, c. 5% Pd:Zn (1:10) /TiO_2 that was calcined at 500°C followed by reduction in 5% H2/Ar at 400°C and d. 5% Pd:Zn(1:10)/Al_2O_3 that was calcined at 500°C followed by reduction in 5% H_2/Ar at 400°C.

TEM analysis

Analysis of particle size distribution was carried out using TEM measurement. Fig 6a shows the TEM image of 5 % Pd/ZnO that was only reduced in H_2 at 400 °C with the histogram of PdZn diameter distribution. The average particle diameter is ~ 6.1 nm. For 5 % Pd/ZnO catalyst that was calcined at 500 °C followed by reduction at 400 °C, the average PdZn diameter obtained was ~ 5.7 nm (Fig 6b). So these catalysts appear to be rather thermally stable. Since the specific surface area of ZnO support that was used is ~ 11 $m^2 g^{-1}$, the dispersion of metal nanoparticles is limited. TiO_2 and Al_2O_3 possess surface areas of 52 $m^2 g^{-1}$ and 100 $m^2 g^{-1}$ respectively, therefore better Pd and Zn nanoparticle distribution should be achieved. TEM images and particle size distribution analysis of 5 % Pd:Zn (1:10)/TiO_2 catalyst are shown in Fig 6c. The catalysts were calcined at 500 °C, followed by reduction at 400 °C. The average diameter is 3.9 nm, which is significantly smaller than for the 5 % Pd/ZnO catalyst. Again these particles appear to be thermally stable. Fig 6d reveals the distribution of PdZn alloy on 5 % Pd:Zn (1:10)/Al_2O_3 with the average particle diameter of 4.9 nm.

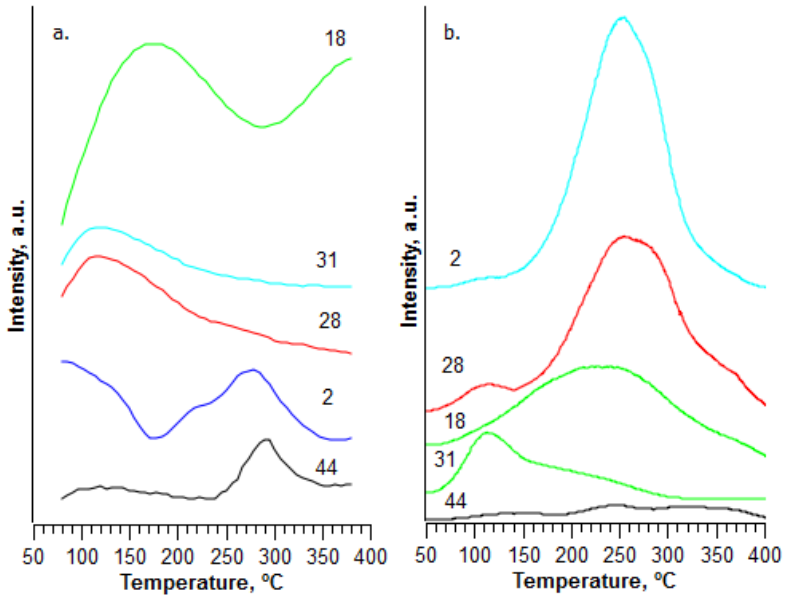

Fig. 7. TPD of a. 5% PdZn/ZnO and b. 5% Pd/TiO_2 saturated with methanol at room temperature. 2 is corresponded to H_2, 18 is corresponded to H_2O, 28 is corresponded to CO, 31 is corresponded to methanol and 44 is corresponded to CO.

TPD studies of methanol on catalyst

In attempt to understand the influence of the PdZn alloy on methanol synthesis, we carried out methanol decomposition studies on 5% Pd/ZnO and 5% Pd/TiO_2 catalysts. The 5% Pd/ZnO catalysts was reduced at 400 °C to form the PdZn alloy. All the catalysts were treated with He at 400°C before dosing with methanol. Fig 7a shows the TPR profiles of methanol decomposition on 5% Pd/ZnO. The catalyst shows coincident CO_2 and H_2 desorption peaks at ~ 280 °C which indicates the decomposition of formate species on the surface. This feature however was negligible on 5% Pd/TiO_2 catalyst (fig.7b).

Catalytic activity

The activity of 5% Pd/ZnO catalysts for CO_2 hydrogenation reaction was investigated and is given in Table 1. The reaction was carried out at 20 bar of pressure and at 250 °C reaction temperature. The catalytic activity of 5 % Pd/ZnO that was only reduced at 400 °C shows ~ 6.7 % conversion of CO_2 to CO at three hours of reaction with ~ 97 % of CO selectivity. The catalyst activity exhibits significant improvement for methanol production when treated in static air for 16 hours at 500 °C before H_2 reduction at 400 °C. The CO_2 conversion increases to 8.7 % and methanol selectivity to 31 % to give 1070 mmol $kg_{cat}^{-1}h^{-1}$ of methanol productivity.

Since it has been established that air-calcination of the catalyst to remove the carbon precursor is crucial for high methanol production, a similar annealing procedure was applied to all the catalysts. Table 1 lists the catalytic activity of the catalysts after 3 h of CO_2 hydrogenation reaction at 250 °C and 20 bar. Catalytic activity of the catalyst was also compared to 5 % Pd/TiO_2 and 5 % Pd/Al_2O_3. 5 % Pd/TiO_2 catalyst gives 6.8 % of CO_2 conversion with 96 % selectivity towards CO. The addition of Zn significantly enhances methanol productivity as was observed on 5% Pd:Zn (1:1)/TiO_2(Table 1). CO_2 conversion increased with increasing zinc content up to Pd:Zn ratio of 1:5 before exhibiting slight reduction at higher Pd:Zn ratios. Similar trends can be seen on 5 % Pd/Al_2O_3 and 5 % Pd:Zn (1:10)/Al_2O_3 catalysts with the addition of Zn significantly improving catalyst activity and methanol yield. CO_2 conversion increases from 0.8 % on 5 % Pd/Al_2O_3 to 8.6 % on 5 % Pd:Zn (1:10)/Al_2O_3 with methanol yield increases from 27.7 mmol $kg_{cat}^{-1}h^{-1}$ to 635 mmol $kg_{cat}^{-1}h^{-1}$ respectively. It is clear that that Zn plays the role of promoter, presumably by producing PdZn active sites to initiate methanol formation. PdZn alloy deposited on TiO_2 showed superior catalytic activity for methanol production from CO_2 hydrogenation.

Effect of reaction temperatures

Further investigation on the activity of the catalyst at lower reaction temperatures was carried out at the range of 200 - 250 °C using the 5% Pd:Zn (1:10)/TiO_2 catalyst. The thermodynamic rules of CO_2 hydrogenation states that increased methanol productivity requires reaction at lower temperature or a higher pressure. It was shown that the selectivity of methanol is higher (~ 94 %) when the reaction was carried out at 200 °C. At this temperature the reaction has 4.2 % CO_2 conversion. The conversion slowly improves with the temperatures up to 250 °C. Methanol productivity is hampered at high reaction temperatures when the rWGS reaction to form CO is favoured. The 5 % Pd:Zn (1:10)/TiO_2 catalyst achieved optimum catalytic activity to methanol at 210 -220 ^oC to give the highest methanol yield of ~ 1700 mmol $kg_{cat}^{-1}h^{-1}$.

Table 1: Catalytic activity of palladium catalysts on ZnO, TiO_2 and Al_2O_3 support.

Catalyst	CO_2 conv, %	CH_3OH sel, %	CO sel, %	CH_3OH productivity mmol $kg_{cat}^{-1}h^{-1}$
5% Pd/ZnO[a]	6.7	2	97	88.20
5% Pd/ZnO	8.2	32	68	1070
5% Pd/TiO_2	6.8	3	96	80.4
5% Pd/Al_2O_3	0.8	7	93	27.7
5% Pd:Zn(1:1)/ TiO_2	7.6	44	55	1420
5% Pd:Zn (1:2)/TiO_2	9.6	38	61	1560
5% Pd:Zn(1:5) /TiO_2	10.1	40	59	1730
5% Pd:Zn(1:10)/TiO_2	6.7	53	46	1510
5% Pd:Zn (1:1) /Al_2O_3				
5% Pd:Zn (1:5) /Al_2O_3	2.4	4	95	38.6
5% Pd:Zn (1:10) /Al_2O_3	3.5	16	83	229
	8.6	19	80	635

[a] Catalyst was only reduced at 400 °C for 3 h without calcination. All the reactions were carried out at 250 °C and 20 bar. 0.5 g of catalysts was used. Data given were measured at 3 hours of reaction.

Discussion

PdZn alloy catalysts with narrow particle size distributions were synthesised using the CVI method. We have modified the work of Forde et.al[26] and Sivakumar et.al[24] which showed that the CVI method can generate nanoparticles with narrow diameters due to the intimate contact between the precursor and support during the sublimation-deposition step. It is likely that the bulky structure of the acetylacetonate ion creates an isolated metal units on the oxide support. As a result, sintering during calcination is reduced and small nanoparticles are produced. Detailed analysis using TEM shows the presence of PdZn nanoparticles with diameters between 1-3 nm on 5 % Pd:Zn (1:10)/TiO_2. The 5 % Pd:Zn (1:10)/TiO_2 catalyst was shown to retain these small nanoparticles despite calcination at 500 °C followed by reduction at 400 °C. It has been reported that catalysts with only of a few metal clusters consisting a 1-10 atoms can dominate the catalytic activity regardless of how big the mean diameter of the metal particles[41, 42]. Studies on Pd metal clusters for CO oxidation reactions showed that clusters containing only 2 Pd atoms increase the CO oxidation dramatically from a monoatomic Pd, but showed a significant drop in activity for 7 Pd atoms catalyst[43]. Studies by Rogers *et al.* on Au nanoparticle catalysts highlighted that the average diameter of metal particles alone does not correlate with catalytic activity; instead, the presence of isolated Au clusters with 1-5 atoms plays a significant role in the catalytic activity for glycerol oxidation[41]. These highlighted that it is important to make a very small alloy particles and CVI is one method to achieve this. The presence of the smallest PdZn alloy with diameter between 1-3 nm could be the most active PdZn alloy in the particle distribution.

Table 2: Catalytic activity of 5 % Pd:Zn (1:10)/TiO_2 at a temperature range of 200 °C to 250 °C.

Reaction temperatures, °C	CO_2conv, %	CH_3OH sel, %	CO sel, %	CH_3OH productivity mmol $kg_{cat}^{-1}h^{-1}$	CO productivity mmol $kg_{cat}^{-1}h^{-1}$
200	4.2	94	5	1620	94.2
210	5.4	80	19	1777	425
220	5.2	80	19	1700	423
230	5.1	78	22	1630	459
240	5.8	63	36	1500	871
250	6.9	53	46	1510	1300

All the reactions were carried out at 250 °C, 20 bar using 0.5 g of catalyst and were pre-treated in 5 % H_2/Ar at 400 °C prior to reaction. Data given were measured at 2 h of reaction.

XPS C 1s analysis and catalytic studies revealed the importance of evacuating most of the carbon from the catalysts structure in order to obtain high activity catalyst for methanol production. In these studies, we introduced Zn during the synthesis in attempt to form PdZn alloy nanoparticles. Introducing Zn with molar ratios of 1Pd:1Zn and upwards on to the Pd/TiO_2 catalyst significantly enhanced methanol productivity from 80.4 mmol $kg_{cat}^{-1}h^{-1}$ to 1730 mmol/ $kg_{cat}^{-1}h^{-1}$, which is also more active than the 5 % Pd/ZnO catalyst. The nature of the active sites in the Pd catalyst for CO_2 hydrogenation provides an insight into the mechanism of the reaction. The Pd catalyst appears to transform into a PdZn alloy under a reductive atmosphere. The PdZn alloy can exist in different compositions with a broader stability region[31], with unique alteration of Pd electronic charges. Rehybridisation of Pd(4d) –Pd(5s,5p) and a charge transfer between Pd(4d) → (Zn(4p) during the formation of Pd-Zn bonds increase the binding energy of the core and valence levels of Pd[30, 44]. This simultaneously reduces the binding energy of core and valence levels of Zn. Pd on TiO_2 and Al_2O_3, for which alloying is unlikely at these treatment temperatures, has been shown to be unreactive for CO_2 hydrogenation to methanol. The insertion of Zn into the Pd lattice creates PdZn alloy, which improves catalyst activity significantly, regardless of the type of metal oxide support used. We believe that the electronic structure alteration of PdZn bimetallic alloy is responsible for its catalytic performance. TPD studies of methanol on 5% Pd/ZnO catalyst (Fig 7a) show the presence of a formate intermediate on the surface by the coincident evolution of CO_2 and H_2 at about 280 °C, whereas without formation of the alloy on 5% Pd/TiO_2 (Fig 7b) this is not evident. It has been shown in the past that formate is the pivotal intermediate which is central to efficient methanol synthesis[30, 45-47]. In turn this implies that changes in the Pd electron density in PdZn, prevents initial C=O bond breakage to make CO and enables the production and stabilisation of the formate intermediate from CO_2 hydrogenation.

The electron perturbation in PdZn alloy exhibits similar electron density of states as metallic Cu[48]. Studies by Neyman et.al indicates that the surface reactivity of PdZn for methanol decomposition was similar to a Cu surface[44]. Formate decomposition on Pd revealed that the formate is very unstable on the Pd surface, decomposing at low temperatures of about -50 °C[49]. In contrast, Cu stabilises the formate up to 200 °C before decomposition to CO_2 and H_2[50]. All the evidence here suggests that the PdZn alloys which are formed improve CO_2 conversion and methanol selectivity. Although the mechanism of the reaction is not fully understood, we believe that the PdZn alloy is able to generate and stabilise the formate intermediate species during CO_2 hydrogenation reaction.

Conclusions

A series of PdZn alloy catalysts were synthesised using chemical vapour impregnation (CVI) to investigate their activity in the CO_2 hydrogenation reaction. Pd on ZnO, TiO_2 and Al_2O_3 has low methanol productivity, though the productivity of the first of these increased enormously upon pre-reduction at high temperature due to the formation of a PdZn alloy. Hence we then produced a series of catalysts in which Pd and Zn were deposited by CVI. The CVI method produced highly dispersed PdZn particles with a mean diameter of 3.9 nm when deposited on TiO_2. The bulky structures of acetylacetonate ion is believed to

be responsible for creating highly isolated Pd and Zn metal species that in turn form the PdZn alloy nanoparticles with a narrow size distribution. Catalytic activity tests revealed the importance of the PdZn alloy phase for stabilizing the formate intermediate and hence a giving high activity for methanol formation from the CO_2 hydrogenation reaction.

Acknowledgements

The authors would like to acknowledge UK Catalysis Hub and EPSRC for research funding to H. Bahruji through grant EP/ I038748/1, W. Jones through EPSRC grant EP/K014714/1, J. Hayward through EU grant.

Notes and references

‡ Footnotes relating to the main text should appear here. These might include comments relevant to but not central to the matter under discussion, limited experimental and spectral data, and crystallographic data.
§
§§
etc.

1. G. A. Olah, G. K. S. Prakash and A. Goeppert, *Journal of the American Chemical Society*, 2011, 133, 12881-12898.
2. S. Lee, *Methanol Synthesis Technology*, Taylor & Francis, 1989.
3. M. Behrens, *Angewandte Chemie International Edition*, 2014, 53, 12022-12024.
4. I. Kasatkin, P. Kurr, B. Kniep, A. Trunschke and R. Schlögl, *Angewandte Chemie*, 2007, 119, 7465-7468.
5. E. I. Solomon, P. M. Jones and J. A. May, *Chemical Reviews*, 1993, 93, 2623-2644.
6. M. Kurtz, N. Bauer, C. Büscher, H. Wilmer, O. Hinrichsen, R. Becker, S. Rabe, K. Merz, M. Driess, R. A. Fischer and M. Muhler, *Catal Lett*, 2004, 92, 49-52.
7. M. Behrens, F. Studt, I. Kasatkin, S. Kühl, M. Hävecker, F. Abild-Pedersen, S. Zander, F. Girgsdies, P. Kurr, B.-L. Kniep, M. Tovar, R. W. Fischer, J. K. Nørskov and R. Schlögl, *Science*, 2012, 336, 893-897.
8. O. Martin, C. Mondelli, D. Curulla-Ferré, C. Drouilly, R. Hauert and J. Pérez-Ramírez, *ACS Catalysis*, 2015, 5, 5607-5616.
9. J. T. Sun, I. S. Metcalfe and M. Sahibzada, *Industrial & Engineering Chemistry Research*, 1999, 38, 3868-3872.
10. N. Iwasa, M. Yoshikawa, W. Nomura and M. Arai, *Applied Catalysis A: General*, 2005, 292, 215-222.
11. N. Iwasa, S. Masuda, N. Ogawa and N. Takezawa, *Applied Catalysis A: General*, 1995, 125, 145-157.
12. H. Bahruji, M. Bowker, G. Hutchings, N. Dimitratos, P. Wells, E. Gibson, W. Jones, C. Brookes, D. Morgan and G. Lalev, *Journal of Catalysis*, 2016, DOI: http://dx.doi.org/10.1016/j.jcat.2016.03.017.
13. C.-H. Kim, J. Lee and D. L. Trimm, *Topics in Catalysis*, 2003, 22, 319-324.
14. X.-L. Liang, X. Dong, G.-D. Lin and H.-B. Zhang, *Applied Catalysis B: Environmental*, 2009, 88, 315-322.
15. H. Zhang, J. Sun, V. L. Dagle, B. Halevi, A. K. Datye and Y. Wang, *ACS Catalysis*, 2014, 4, 2379-2386.
16. L. Fan and K. Fujimoto, *Journal of Catalysis*, 1994, 150, 217-220.
17. S. E. Collins, J. J. Delgado, C. Mira, J. J. Calvino, S. Bernal, D. L. Chiavassa, M. A. Baltanás and A. L. Bonivardi, *Journal of Catalysis*, 2012, 292, 90-98.
18. T. Fujitani, M. Saito, Y. Kanai, T. Watanabe, J. Nakamura and T. Uchijima, *Applied Catalysis A: General*, 1995, 125, L199-L202.
19. J. Qu, X. Zhou, F. Xu, X.-Q. Gong and S. C. E. Tsang, *The Journal of Physical Chemistry C*, 2014, 118, 24452-24466.
20. Z. Zsoldos, A. Sarkany and L. Guczi, *Journal of Catalysis*, 1994, 145, 235-238.
21. M. Behrens, F. Studt, I. Kasatkin, S. Kühl, M. Hävecker, F. Abild-Pedersen, S. Zander, F. Girgsdies, P. Kurr, B.-L. Kniep, M. Tovar, R. W. Fischer, J. K. Nørskov and R. Schlögl, *Science*, 2012, 336, 893-897.
22. F. Studt, M. Behrens, E. L. Kunkes, N. Thomas, S. Zander, A. Tarasov, J. Schumann, E. Frei, J. B. Varley, F. Abild-Pedersen, J. K. Nørskov and R. Schlögl, *ChemCatChem*, 2015, 7, 1105-1111.
23. B. Sakakini, J. Tabatabaei, M. J. Watson, K. C. Waugh and F. W. Zemicael, *Faraday Discussions*, 1996, 105, 369-376.
24. P. Sivakumar, R. Ishak and V. Tricoli, *Electrochimica Acta*, 2005, 50, 3312-3319.
25. V. Dal Santo, C. Mondelli, V. De Grandi, A. Gallo, S. Recchia, L. Sordelli and R. Psaro, *Applied Catalysis A: General*, 2008, 346, 126-133.
26. M. M. Forde, L. Kesavan, M. I. bin Saiman, Q. He, N. Dimitratos, J. A. Lopez-Sanchez, R. L. Jenkins, S. H. Taylor, C. J. Kiely and G. J. Hutchings, *ACS Nano*, 2014, 8, 957-969.
27. http://www.casaxps.com/.
28. http://maud.radiographema.com/.
29. P. S. Wehner, G. C. Tustin and B. L. Gustafson, *Journal of Catalysis*, 1984, 88, 246-248.
30. J. A. Rodriguez, *The Journal of Physical Chemistry*, 1994, 98, 5758-5764.
31. J. Vizdal, A. Kroupa, J. Popovic and A. Zemanova, *Advanced Engineering Materials*, 2006, 8, 164-176.
32. G. Deroubaix and P. Marcus, *Surface and Interface Analysis*, 1992, 18, 39-46.
33. W. Li, L. Fang, G. Qin, H. Ruan, H. Zhang, C. Kong, L. Ye, P. Zhang and F. Wu, *Journal of Applied Physics*, 2015, 117, 145301.
34. M. L. Cubeiro and J. L. G. Fierro, *Applied Catalysis A: General*, 1998, 168, 307-322.
35. A. Bayer, K. Flechtner, R. Denecke, H.-P. Steinrück, K. M. Neyman and N. Rösch, *Surface Science*, 2006, 600, 78-94.
36. L. S. Dake, D. R. Baer and J. M. Zachara, *Surface and Interface Analysis*, 1989, 14, 71-75.
37. S. Kuld, C. Conradsen, P. G. Moses, I. Chorkendorff and J. Sehested, *Angewandte Chemie International Edition*, 2014, 53, 5941-5945.
38. V. Schott, H. Oberhofer, A. Birkner, M. Xu, Y. Wang, M. Muhler, K. Reuter and C. Wöll, *Angewandte Chemie International Edition*, 2013, 52, 11925-11929.
39. N. S. Babu, N. Lingaiah, N. Pasha, J. V. Kumar and P. S. S. Prasad, *Catalysis Today*, 2009, 141, 120-124.
40. V. A. d. l. P. O'Shea, M. C. Álvarez-Galván, J. L. G. Fierro and P. L. Arias, *Applied Catalysis B: Environmental*, 2005, 57, 191-199.
41. S. M. Rogers, C. R. A. Catlow, C. E. Chan-Thaw, D. Gianolio, E. K. Gibson, A. L. Gould, N. Jian, A. J. Logsdail, R. E. Palmer, L. Prati, N. Dimitratos, A. Villa and P. P. Wells, *ACS Catalysis*, 2015, 5, 4377-4384.
42. A. A. Herzing, C. J. Kiely, A. F. Carley, P. Landon and G. J. Hutchings, *Science*, 2008, 321, 1331-1335.
43. E. C. Tyo and S. Vajda, *Nat Nano*, 2015, 10, 577-588.
44. K. M. Neyman, K. H. Lim, Z.-X. Chen, L. V. Moskaleva, A. Bayer, A. Reindl, D. Borgmann, R. Denecke, H.-P. Steinruck and N. Rosch, *Physical Chemistry Chemical Physics*, 2007, 9, 3470-3482.
45. M. Bowker, H. Houghton and K. C. Waugh, *Journal of the Chemical Society, Faraday Transactions 1: Physical Chemistry in Condensed Phases*, 1981, 77, 3023-3036.
46. M. Bowker, *Vacuum*, 1983, 33, 669-685.
47. M. Bowker, R. A. Hadden, H. Houghton, J. N. K. Hyland and K. C. Waugh, *Journal of Catalysis*, 1988, 109, 263-273.
48. A. Pang Tsai, S. Kameoka and Y. Ishii, *Journal of the Physical Society of Japan*, 2004, 73, 3270-3273.
49. N. Aas, L. Yongxue and M. Bowker, *Journal of Physics: Condensed Matter*, 1991, 3, S281.
50. M. Bowker and R. J. Madix, *Surface Science*, 1981, 102, 542-565.